

# Mathematical Modeling of the Contact Interaction of the Fuel Element Section, Including up to 100 Pellets, Taking into Account Creep

PAVEL ARONOV<sup>1,2</sup>, MIKHAIL GALANIN<sup>1,2</sup>, ALEXANDR RODIN<sup>1,2</sup>

<sup>1</sup>Keldysh Institute of Applied Mathematics (Russian Academy of Sciences)

Miuskaya sq., 4 Moscow, 125047

RUSSIA

<sup>2</sup>Bauman Moscow State Technical University

Baumanskaya 2-ya st., 5/1, Moscow, 105005

RUSSIA

*Abstract:* An algorithm for solving axisymmetric contact problems of thermoelasticity taking into account creep processes is considered. To account for the contact interaction of bodies, the mortar method was used, and the modified Jacobi method was used to solve the resulting system of linear equations. For the numerical solution of the problem simulating the creep process, time discretization based on the implicit Euler method was applied, and the Newton method was used to linearize the resulting system of equations. An algorithm with automatic step selection based on obtaining an estimate of the local error of the method is proposed. The results of applying the proposed algorithm to a demonstration problem simulating thermomechanical processes in a section of a fuel element comprising from 1 to 100 fuel pellets are presented.

*Key-Words:* contact problem of the thermoelasticity theory, finite element method, mortar method, creep, fuel element

Received: March 29, 2022. Revised: April 15, 2022. Accepted: May 14, 2022. Published: July 4, 2022.

## 1 Introduction

Taking into account the contact interaction of various functional components of the equipment is an important component in assessing the stress-strain state of most structures. It is impossible to obtain an analytical solution for practically important contact problems, and numerical methods are used to determine the displacement and stress fields. Therefore, the problem of creating new effective algorithms and modern application software based on them for solving contact problems of computational thermomechanics is urgent. The numerical solution of such problems can be carried out using the domain decomposition method [1], the penalty method [2], various variants of the Lagrange multiplier method [3], in particular, the mortar method [4].

The paper presents the formulation of a quasi-stationary multicontact problem and presents an algorithm for the numerical solution of such problems taking into account changes in time of deformations and stresses due to the creep effect. The application of the proposed algorithm to a problem simulating processes in a section of a fuel element operating in the mode of constant heat dissipation power is considered. To ac-

count for the creep effect, an algorithm based on the implicit Euler method in combination with the Newton method for linearization is considered. Calculations with constant and variable time steps were carried out and the results obtained were compared.

## 2 Mathematical formulation of the problem

Let us limit ourselves to solving the following axisymmetric problem simulating thermomechanical processes occurring in a fuel element: inside the cylindrical cladding  $G_N$  there is a column of  $N - 1$  identical cylindrical pellets  $G_1, \dots, G_{N-1}$  stacked on top of each other, having an inner hole and chamfers at both ends. Fig. 1 shows the modeling area corresponding to half of the longitudinal section of the fuel element section. We introduce the following notation for the surfaces of bodies:  $S_1$  is the surface area on which the 1st kind condition for the normal displacement component is set,  $S_2$  is the inner surface of the pellets,  $S_3$  is the upper end of the upper pellet,  $S_4$  is the outer surface of pellets,  $S_5$  is the inner surface of the cladding,  $S_6$  is the outer surface of the cladding.

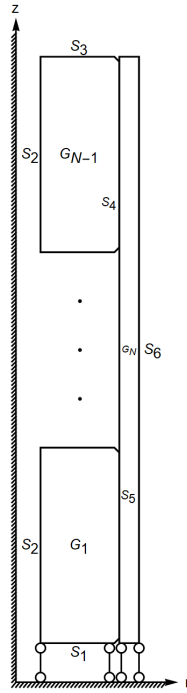


Figure 1: Scheme of the area model

Suppose that the coupling effect can be neglected, so we will solve the problem of thermal conductivity separately, and use the resulting temperature field to solve the contact problem of thermomechanics. When solving the thermal conductivity equation, the influence of the resulting mechanical deformations is not taken into account.

Consider the following initial boundary value problem for a nonlinear heat equation in the domain  $G = \bigcup_{\alpha=1}^N G_{\alpha}, t > 0$  [5]:

$$c(T)\rho \frac{\partial T}{\partial t} = (k_{ij}(T)T_{,j})_{,i} + q(\mathbf{x}, t), \quad \mathbf{x} \in G; \quad (1)$$

$$T(\mathbf{x}, 0) = T_0(\mathbf{x}), \quad \mathbf{x} \in G; \quad (2)$$

$$T(\mathbf{x}, t) = T_1(\mathbf{x}), \quad \mathbf{x} \in S_6; \quad (3)$$

$$-n_i k_{ij}(T)T_{,j}(\mathbf{x}, t) = 0, \quad \mathbf{x} \in \partial G_p \setminus S_4; \quad (4)$$

$$-n_i k_{ij}(T)T_{,j}(\mathbf{x}, t) = \alpha [T(\mathbf{x}, t) - T_f(\bar{\mathbf{x}}, t)], \quad \mathbf{x} \in S_4, \quad \bar{\mathbf{x}} \in S_5, \quad (5)$$

where  $c(T)$  is the specific mass heat capacity of the medium,  $\rho$  is density of the medium,  $\mathbf{x}$  is a vector of spatial coordinates,  $t$  is time,  $k_{ij}$  are the components of the thermal conductivity tensor,  $T_{,j} = \frac{\partial T}{\partial x_j}$ ,  $q(\mathbf{x}, t)$  is the power of internal heat sources (different from zero in pellets),  $T_0(\mathbf{x})$  is initial temperature,  $T_1(\mathbf{x}, t)$  is surface temperature  $S_6$ ,  $T(\mathbf{x}, t)$  is temperature at

time  $t$ ,  $n_i$  are the components of the unit vector of the external normal to the boundary  $\partial G$ ,  $\alpha$  is the heat transfer coefficient on the surfaces  $S_4$  and  $S_5$ ,  $T_f(\mathbf{x})$  is temperature at a similar point lying on the inner surface of the cladding.

The mathematical formulation of the quasi-stationary problem of deformable solid mechanics for the case when there are no volumetric forces includes [5] the following relations for each body with the number  $\alpha$  ( $i, j = \overline{1, 3}$ ),  $t > 0$ :

- equilibrium equations

$$\sigma_{ji,j}(\mathbf{u}, t) = 0, \quad \mathbf{x} \in G_{\alpha}; \quad (6)$$

- kinematic boundary conditions

$$\mathbf{u}(\mathbf{x}, t) = \mathbf{u}_0(\mathbf{x}, t), \quad \mathbf{x} \in S_D; \quad (7)$$

- force boundary conditions

$$\sigma_{ji}(\mathbf{u}, t)n_j = p_i(\mathbf{x}, t), \quad \mathbf{x} \in S_N; \quad (8)$$

- Cauchy relations for a linear full strain tensor

$$\varepsilon_{ij}(\mathbf{x}, t) = \frac{1}{2}(u_{i,j}(\mathbf{x}, t) + u_{j,i}(\mathbf{x}, t)), \quad \mathbf{x} \in G_{\alpha}; \quad (9)$$

- defining equations (Hooke's law)

$$\sigma_{ij}(\mathbf{x}, t) = C_{ijkl}(\varepsilon_{kl}(\mathbf{x}, t) - \varepsilon_{kl}^0(\mathbf{x}, t)), \quad \mathbf{x} \in G_{\alpha}, \quad (10)$$

where  $x_i$  are the coordinates of the vector  $x \in G_{\alpha}$ ;  $\sigma_{ij}$  are the components of the stress tensor;  $\varepsilon_{kl}$  are the components of the full strain tensor;  $\varepsilon_{kl}^0$  are the components of the inelastic strain tensor;  $u_i$  are the components of the displacement vector;  $C_{ijkl}$  are the components of the tensor of elastic constants;  $p_i$  are the components of the vector of surface forces;  $n_j$  are the components of the vector of the external normal to the corresponding surface  $S_j$ ;  $S_D$  and  $S_N$  is the union of surfaces on which kinematic and force boundary conditions are set, respectively.

In the calculations carried out, it was assumed that the lower ends of the cladding and the lower pellet are fixed vertically,  $p_i(\mathbf{x})$  differs from zero only on the upper end of the upper pellet  $S_3^{N-1}$  (constant pressure 50 MPa) and on the outer surface of the cladding  $S_4^N$  (constant pressure 10 MPa). The model took into account that each pellet (except  $G_1$  and  $G_{N-1}$ ) comes into contact with two adjacent (top and bottom) pellets and the cladding (it is assumed that there is no initial gap between them). Thus, there are  $N - 2$  pellet/pellet contact pairs ( $S_1^{\alpha}, S_3^{\alpha+1}$ ) and  $N - 1$  pellet/cladding

contact pairs  $(S_4^\alpha, S_2^N)$ . Sliding conditions without friction are set on the contact surfaces.

Consider a pair of potentially contact surfaces related to bodies with numbers  $\alpha_1$  and  $\alpha_2$ . To simplify the record, we will use the index "1" instead of " $\alpha_1$ " and "2" instead of " $\alpha_2$ ". For pellet/pellet contact pairs, the index "1" denotes the upper end of the lower pellet, and the index "2" denotes the lower end of the upper pellet, and for pellet/cladding contact pairs, the index "1" denotes the outer surface of the pellet, and the index "2" denotes the inner surface of the cladding. Then the additional conditions on the surface  $S_k^1$  for the case of frictionless contact are as follows (for the surface  $S_k^2$  conditions are written in the same way):

$$\sigma_\tau^1(\mathbf{x}_1) = 0; \quad (11)$$

$$\sigma_n^1(\mathbf{x}_1) = \sigma_n^2(\bar{\mathbf{x}}_2) \leq 0; \quad (12)$$

$$u_n^1(\mathbf{x}_1) + u_n^2(\bar{\mathbf{x}}_2) \leq \delta_{0n}(\mathbf{x}_1); \quad (13)$$

$$\sigma_n^1(\mathbf{x}_1) (u_n^1(\mathbf{x}_1) + u_n^2(\bar{\mathbf{x}}_2) - \delta_{0n}(\mathbf{x}_1)) = 0. \quad (14)$$

Here  $\mathbf{x}_1$  is a some point lying on the surface of  $S_k^1$ , and  $\bar{\mathbf{x}}_2$  is a similar point, i.e. located opposite (normal to  $S_k^1$ ) the point  $\mathbf{x}_1$  on the surface of  $S_k^2$ ,  $\delta_{0n}(\mathbf{x}_1) \geq 0$  is the function that sets the initial gap (the surface areas could not touch each other at the initial moment),  $u_n^\alpha = \mathbf{u}^\alpha \cdot \mathbf{n}^\alpha$ ,  $\sigma_\tau^\alpha = (\sigma(\mathbf{u}^\alpha) \cdot \mathbf{n}^\alpha) \cdot \boldsymbol{\tau}^\alpha$ ,  $\sigma_n^\alpha = (\sigma(\mathbf{u}^\alpha) \cdot \mathbf{n}^\alpha) \cdot \mathbf{n}^\alpha$ .

The conditions (11)–(14) guarantee that if  $S_k^1$  and  $S_k^2$  coincide (in advance, the configuration and position of this section unknown), then compressive contact forces will act on the contacting areas. The conditions (11)–(12) are forceful, the condition (13) is kinematic.

These conditions describe two possible situations: 1) in the final configuration, sections of potentially contacting surfaces are in contact, kinematic conditions (the corresponding coordinates coincide) and force conditions (contact pressure modules coincide) are met or 2) areas of potentially contacting surfaces are not in contact: there is a gap between them, contact pressures are equal to 0.

A characteristic feature of the considered problem is that it considers many contact pairs, while there is a strong change in the configuration of the contact surfaces during the operation of the fuel element. For each pellet/pellet contact pair, as a result of heating, a significant number of grid nodes located closer to the chamfer come out of contact. Due to the large length of the structure along the  $z$  axis, the fuel pellets, especially in the upper part of the column, are displaced by a considerable distance relative to their initial position (and relative to the cladding).

To simulate the creep process, we will use the flow theory, the main provisions of which include [6]:

- additive decomposition of the derivative of the full strain tensor in time

$$\dot{\varepsilon}_{ij} = \dot{\varepsilon}_{ij}^e + \dot{\varepsilon}_{ij}^T + \dot{\varepsilon}_{ij}^c; \quad (15)$$

- incompressibility of creep deformation

$$\dot{\varepsilon}_{ii}^c = 0; \quad (16)$$

- the relation for the derivative of the creep strain tensor in time

$$\dot{\varepsilon}_{ij}^c = \mu \sigma'_{ij}, \quad (17)$$

where  $\mu = \frac{1}{2} \frac{\dot{\varepsilon}_i^c}{\sigma_i}$ ,  $\sigma_i = \sqrt{\frac{3}{2} \sigma'_{kl} \sigma'_{kl}}$ ,  $\dot{\varepsilon}_i^c = f(T, \sigma_i)$ ,  $\sigma'_{kl} = \sigma_{kl} - \frac{1}{3} \sigma_{jj} \delta_{kl}$ .

Solving the problem (6)–(10) at time  $t_m$  is equivalent to [7] minimizing the functional

$$\begin{aligned} \Pi = & \frac{1}{2} \int_{G_\alpha} \boldsymbol{\sigma}^T (\boldsymbol{\varepsilon} - \boldsymbol{\varepsilon}^0) dG - \int_{S_N} \mathbf{u}^T \mathbf{p} dS + \\ & + \int_{S_k} \lambda_n (u_{2n}(\mathbf{x}) + u_{1n}(\mathbf{x}) - \delta_{0n}) dS \end{aligned} \quad (18)$$

when the kinematic boundary conditions (7) are met, where  $\lambda_n$  —Lagrange multipliers that are projections of stress vectors on the directions of external normals,  $u_n = u_r n_r + u_z n_z$ .

For spatial discretization of the functional (18), the finite element method was used, second-order elements on a quadrangular grid were used in calculations. The discretization of the integral over the contact surfaces is performed using the mortar method [8], which is the variant of the Lagrange multiplier method for the case of inconsistent meshes. The algorithm and some features of the application of the mortar method are described in [9].

The choice of the most effective method for solving systems of linear equations arising during the discretization of the problem was carried out. For this purpose, the contact problem was solved in a thermoelastic formulation for a large number of pellets (up to 100). The use of modified iterative methods (in particular, the modified Jacobi method) turned out to be more effective than the use of standard methods for solving systems of linear equations (for example, the Gauss method for sparse matrices or GMRES). The selected preconditioner [9] enables us to automatically take into account the exit from the contact without additional intervention in the algorithm.

Since stresses depend on creep deformations, the equation (17) can be represented as the following system of ordinary differential equations in vector form:

$$\dot{\varepsilon}^c = \mathbf{f}(\varepsilon^c, t). \quad (19)$$

If the implicit Euler method is used to solve (19), then at time  $t_{m+1}$  the formulas for the local vector are valid (for the element with the number  $(e)$ ) increments of creep strain and local stress vector

$$\begin{aligned} \Delta \varepsilon^{c(e)} &= \varepsilon^{c(e)}(t_{m+1}) - \varepsilon^{c(e)}(t_m) = \\ &= \tau_m \mu(t_{m+1}) \sigma^{l(e)}(t_{m+1}); \end{aligned} \quad (20)$$

$$\begin{aligned} \sigma^{(e)}(t_{m+1}) &= D^{(e)}(\varepsilon^{(e)}(t_{m+1}) - \varepsilon^{T(e)}(t_{m+1}) - \\ &- \varepsilon^{c(e)}(t_m) - \Delta \varepsilon^{c(e)}), \end{aligned} \quad (21)$$

where  $D^{(e)}$  is the elasticity matrix. The equation (18) is nonlinear, the Newton method is used for linearization [10].

The numerical algorithm can be described as follows:

1. For the moment of time  $t_{m+1}$ , at the iteration with the number  $i + 1$ , after summing local vectors and matrices into global ones, the following system of linear algebraic equations is solved using a modified Jacobi method [9]

$$\begin{pmatrix} \mathbf{K}^i(t_{m+1}) & \mathbf{M}^l \\ \mathbf{M}^{lT} & \mathbf{0} \end{pmatrix} \begin{pmatrix} \Delta \mathbf{u}^{i+1} \\ \Delta \boldsymbol{\lambda}^{i+1} \end{pmatrix} = \begin{pmatrix} \mathbf{R}(t_{m+1}) \\ \mathbf{0} \end{pmatrix} \quad (22)$$

where  $\Delta \mathbf{u}^{i+1} = \mathbf{u}^{i+1}(t_{m+1}) - \mathbf{u}^i(t_{m+1})$  is the vector of increment of displacements per iteration,  $\Delta \boldsymbol{\lambda}^{i+1} = \boldsymbol{\lambda}^{i+1}(t_{m+1}) - \boldsymbol{\lambda}^i(t_{m+1})$  is the vector of increments of Lagrange multipliers per iteration, the matrix  $\mathbf{M}^l$  reflects the contribution of the contact surface integral to (18), the matrix  $\mathbf{K}^i$  takes into account the contribution of temperature deformation and creep deformation, it is calculated anew at each iteration and has the following structure [10]:

$$\mathbf{K}^i = \begin{pmatrix} c_1 & c_2 & c_2 & 0 \\ c_2 & c_1 & c_2 & 0 \\ c_2 & c_2 & c_1 & 0 \\ 0 & 0 & 0 & c_3 \end{pmatrix}, \quad (23)$$

where  $c_1 = \frac{1}{3}(2C' + C_m)$ ,  $c_2 = \frac{1}{3}(C_m - C')$ ,  $c_3 = \frac{1}{2}C'$ ,  $C' = \frac{1}{a_E + \tau_k \varepsilon^c}$ ,  $C_m = \frac{E}{1 - 2\nu}$ ,  $a_E = \frac{1 + \nu}{E}$ ,  $\tau_m = t_{m+1} - t_m$ .

2. For each finite element with index  $(e)$  by displacement values in nodes  $\mathbf{u}^{(i+1)(e)}(t_{m+1})$  the deformation vector  $\varepsilon^{(i+1)(e)}(t_{m+1})$  and the stress vector are calculated as follows:

$$\begin{aligned} \sigma^{(i+1)(e)}(t_{m+1}) &= \mathbf{D}^{(e)}(\varepsilon^{(i+1)(e)}(t_{m+1}) - \\ &- \varepsilon^{T(e)}(t_{m+1}) - \varepsilon^{c(i)(e)}(t_{m+1})). \end{aligned} \quad (24)$$

3. The formula (20) calculates the values of  $\Delta \varepsilon^{c(i+1)(e)}$  and new creep strain values are found:

$$\varepsilon^{c(i+1)(e)}(t_{m+1}) = \varepsilon^{c(e)}(t_m) + \Delta \varepsilon^{c(i+1)(e)}. \quad (25)$$

4. The convergence of the iterative process within the time step under consideration is estimated: if the following inequality holds

$$\max_{1en} \|\varepsilon^{c(i+1)(e)}(t_{m+1}) - \varepsilon^{c(i)(e)}(t_{m+1})\| < \delta, \quad (26)$$

where  $\delta$  is the specified accuracy, then there is a transition to the next time step (if the specified time interval has not yet been passed ( $t_{m+1} < t_{end}$ )), otherwise — to the next iteration.

To automatically select the length of the time step at time  $t_{m+1}$ , we will use the following algorithm [11], based on Richardson extrapolation:

$$\tau_{new} = \tau \cdot \min \left( f_1, \max \left( f_2, f_3 \cdot \left( \frac{tol}{err} \right)^{\frac{1}{p+1}} \right) \right), \quad (27)$$

where  $f_3$  is the guarantee coefficient,  $f_1, f_2$  are the coefficients that ensure not too fast increase or decrease of the step, in this case  $p = 1$  is the order of accuracy of the explicit and implicit Euler method,  $tol$  is the required level of accuracy. The implicit Euler method is A-stable, so when choosing the step length, one only needs to follow the approximation of the data [11].

The estimation of the local relative error for the moment of time  $t_{m+1}$  is carried out as follows:

$$err = \frac{1}{2^p - 1} \max_j \left\| \frac{\hat{\varepsilon}_j^c - \varepsilon_j^c}{\varepsilon_j^c} \right\|_2 \quad (28)$$

where  $\hat{\varepsilon}_j^c(t_{m+1})$  is the component of the global creep strain vector obtained after from the time point  $t_{m-1}$  the calculation was performed for one time step of length  $2\tau$ ,  $\varepsilon_j(t_{m+1})$  is the component of the global creep strain vector obtained after from the point  $t_{m-1}$  the calculation is performed for two time steps of length  $\tau$ . If  $err \leq tol$ , then the resulting values are  $\varepsilon_j(t_{m+1})$  are accepted and a new calculation cycle is performed from the point  $t_{m+1}$ : 2 time steps of length  $\tau_{new}$  and one time step of length  $2\tau_{new}$ . If  $err > tol$ , then the resulting values are  $\varepsilon_j(t_{m+1})$  are considered rejected, there is a return to the point  $t_{m-1}$  and a new calculation cycle is performed, taking into account that  $\tau_{new} < \tau$ .

### 3 Results of the numerical solution

We will carry out a series of calculations for the fuel element section, which includes from 1 to 100 fuel pellets. The inner radius of the pellets is 0.8 mm, the outer radius is — 3.88 mm, the height is — 10 mm, the outer radius of the cladding is 4.55 m [12]. We will consider inconsistent grids: pellets are divided into 10 elements in the directions of  $r$  and  $z$ , and the cladding — into 5 elements in the direction of  $r$ , in the direction of  $z$ , each section of the cladding corresponding to the height of one pellet is divided into 10 elements. The average fuel element usage time in the reactor is several years, so let's choose the calculation time  $t_{end} = 3.2 \cdot 10^8$  c ( $\approx 10$  years).

Let us consider the creep models used for the materials of fuel pellets and claddings, which are elements of the fuel element. The pellets are made of uranium dioxide, the cladding is made of zirconium alloy. Let's give these models in more detail, described in [13].

The rate of stationary creep deformation for fuel pellets is determined by the expression:

$$\begin{aligned} \dot{\varepsilon}_i^c = & \frac{(A_1 + A_2 F) \sigma e^{-\frac{Q_1}{RT}}}{(A_3 + D) G^2} + \\ & + \frac{(A_4 + A_7 F) \sigma^{4.5} e^{-\frac{Q_2}{RT}}}{A_5 + D} + A_6 \sigma F e^{-\frac{Q_3}{RT}}, \quad (29) \end{aligned}$$

where  $\dot{\varepsilon}_i^c$  is the rate of stationary creep deformation (1/s),  $F$  is the density of divisions ((divisions/m<sup>3</sup>)/c),  $\sigma$  is the stress (Pa),  $R$  — universal gas constant (Cal/(mol K)),  $T$  is temperature (K),  $D$  is density (percentage of theoretical density),  $Q_1, Q_2, Q_3$  is activation energy (Cal/mol),  $A_1, \dots, A_7$  are the constant coefficients.

For the cladding, the rate of steady-state creep deformation has the form:

$$\begin{aligned} \dot{\varepsilon}_i^c = & \frac{(B_1 + B_2 F) \sigma}{(A_3 + D) G^2} e^{-\frac{Q_4}{RT} + B_3(1-D) + B_4 C} + \\ & + \frac{(B_5 + B_6 F) \sigma}{(A_3 + D) G^2} e^{-\frac{Q_5}{RT} + B_7(1-D) + B_4 C}, \quad (30) \end{aligned}$$

where  $Q_4, Q_5$  is activation energy (Cal/mol),  $C$  is the concentration of oxide mixture (weight percentage),  $G$  is the fuel pellet size (cm),  $B_1, \dots, B_7$  are the constant coefficients.

Graphs of the dependences of displacements and stresses at the contact boundaries, as well as their two-dimensional distributions in pellets and claddings are presented in [12].

Fig. 2 shows two-dimensional radial, axial and circumferential stress distributions for pellets, and

Fig. 3 shows similar distributions for the cladding at the final moment of time. Fig. 4 shows two-dimensional distributions of radial, axial and circumferential creep deformations for pellets, and Fig. 5 shows similar distributions for the cladding. Fragments of distributions corresponding to the section from the 5th to the 9th pellets are shown, and when constructing deformed bodies, the applied displacements are increased 10 times for pellets and 50 times for the cladding for greater clarity. It can be seen from the graphs presented that radial stresses are compressive in almost the entire pellet, the greatest compressive stresses are achieved in the center of the pellets. The greatest axial and circumferential stresses are observed at the outer surface of the pellets, the smallest stresses occur at the inner surface.

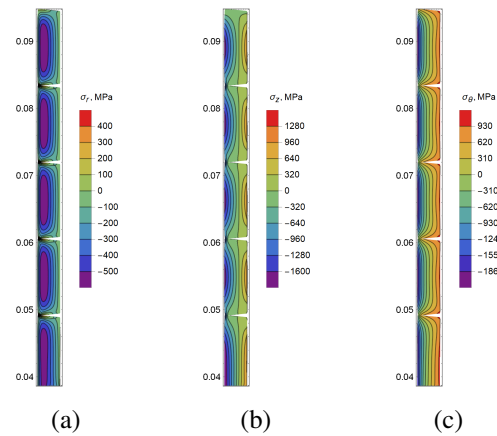


Figure 2: Two-dimensional distributions in the nodes of pellet elements for the moment of time  $t = 3, 2 \cdot 10^8$  s: a — radial stresses; b — axial stresses; c — circumferential stresses

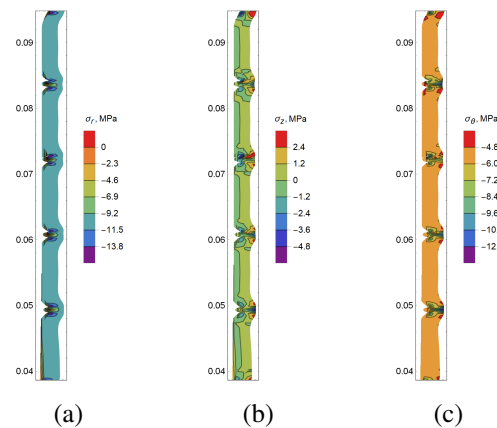


Figure 3: Two-dimensional distributions in the nodes of the cladding elements for the moment of time  $t = 3, 2 \cdot 10^8$  s: a — radial stresses; b — axial stresses; c — circumferential stresses

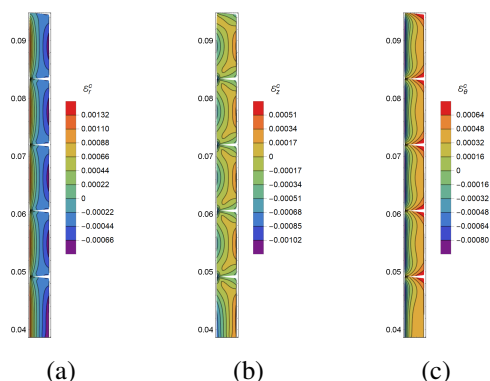


Figure 4: Two-dimensional distributions in the nodes of pellet elements for the moment of time  $t = 3,2 \cdot 10^8$  s: a — radial creep deformations; b — axial creep deformations; c — circumferential creep deformations

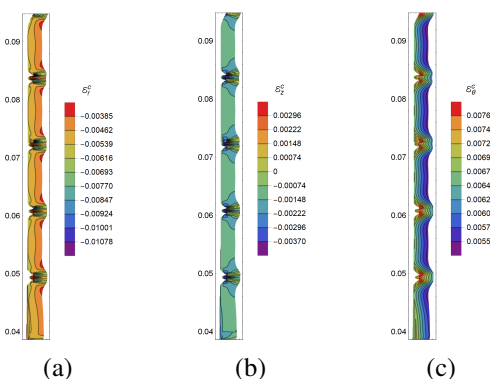


Figure 5: Two-dimensional distributions in the nodes of the cladding elements for the moment of time  $t = 3,2 \cdot 10^8$  s: a — radial creep deformations; b — axial creep deformations; c — circumferential creep deformations

Fig. 6, Fig. 7 shows graphs of the dependences of the average values of radial stresses on the outer surface of fuel pellets for the case of 100 pellets (one point corresponds to one pellet) at various points in time. The heat dissipation power is constant (Fig. 6) or varies according to the sinusoidal law according to the height of the fuel column (Fig. 7). It can be seen from the above graphs that radial stresses decrease 5–10 times over 10 years compared to the initial stresses in the structure. Thus, taking into account creep deformations leads to a noticeable decrease in stress values in the structure.

In Fig. 8, Fig. 9 graphs of the average values of radial and axial displacements on the outer surface of pellets are presented (one point corresponds to one pellet, the total number is 100 pellets) for cases of constant and sinusoidal heat dissipation power at various

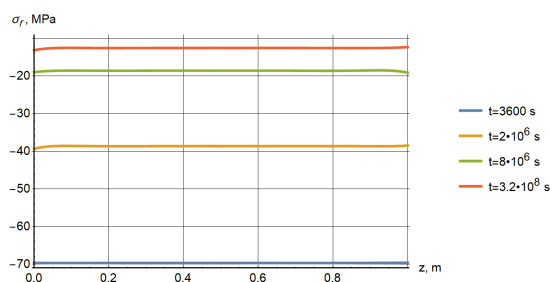


Figure 6: Dependences of the average values of the radial stress  $\sigma_r(z)$  at  $r = 0.0038$  m: constant heat dissipation power

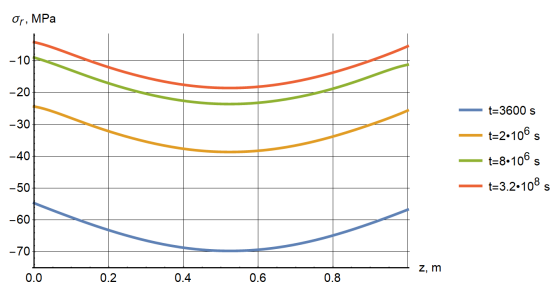


Figure 7: Dependences of the average values of the radial stress  $\sigma_r(z)$  at  $r = 0.0038$  m: sinusoidal heat dissipation power

points in time. As can be seen from the figures, there is a significant displacement of the column of fuel pellets relative to the initial position (up to 1.5 cm, which is comparable to the height of the pellet).

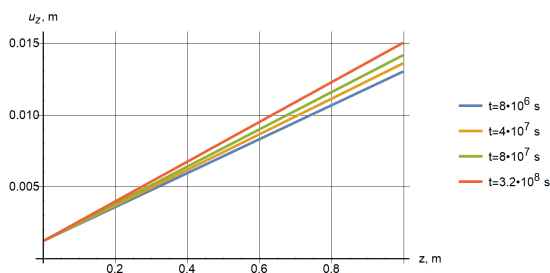


Figure 8: Dependences of the average values of the axial displacement  $u_z(z)$  at  $r = 0.0038$  m: constant heat dissipation power

The Table 1 shows constant and maximum time steps for a different number of pellets and  $tol = 10^{-4}$ , the Table 2 shows calculation time and number of steps, and the Table 3 shows errors in calculations with a variable step relative to calculations with a constant step.

Fig. 10 and Fig.11 show graphs of the dependencies of

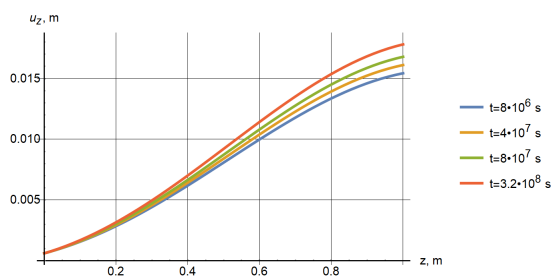


Figure 9: Dependences of the average values of the axial displacement  $u_z(z)$  at  $r = 0.0038$  m: sinusoidal heat dissipation power

Table 1: Constant and maximum time steps

Number of pellets	Const. time step	Max. time step
1 pellet	$2 \cdot 10^5$ s	$2,37 \cdot 10^7$ s
2 pellets	$5 \cdot 10^4$ s	$1,09 \cdot 10^7$ s
5 pellets	$2 \cdot 10^4$ s	$7,56 \cdot 10^6$ s
10 pellets	$1,5 \cdot 10^3$ s	$3,69 \cdot 10^6$ s
25 pellets	750 s	$1,24 \cdot 10^6$ s
50 pellets	250 s	$5,31 \cdot 10^5$ s
100 pellets	—	$2,25 \cdot 10^5$ s

the  $\tau$  step and estimates of the local relative error  $err$  from time to time for the case of 25 pellets and a given accuracy  $tol = 10^{-4}$ . The figures show how the time step  $\tau$  changes and that  $err$  does not exceed the value of  $tol$  throughout the calculation.

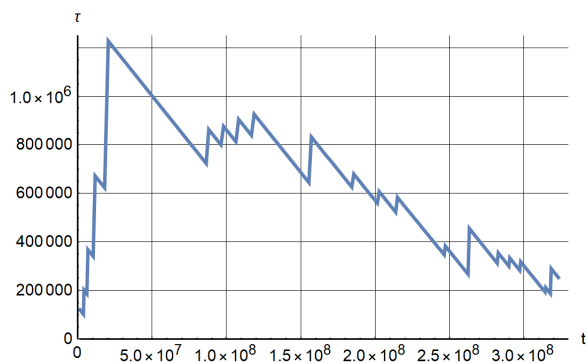


Figure 10: Dependences of the  $\tau$  step from time for 25 pellets

From the results given in the Table 2, it can be seen that when using a variable time step, it is possible to reduce the calculation time by 10–15 times compared to the calculation with a constant step (10

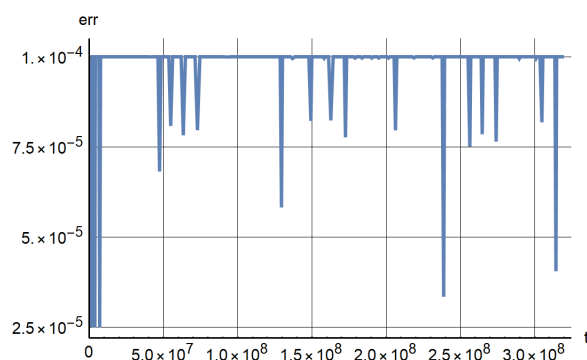


Figure 11: Dependences of  $err$  from time for 25 pellets

Table 2: Calculation time and number of time steps

Number of pellets	Const. time step	Max. time step
1 pellet	91,4 s 1600 steps	10,9 s 30 steps
2 pellets	122,6 s 6400 steps	23,1 s 52 steps
5 pellets	1623,9 s 16000 steps	134,7 s 85 steps
10 pellets	10075,5 s 213333 steps	664,7 s 176 steps
25 pellets	—	3327,6 s 450 steps
50 pellets	—	9213,2 s 911 steps
100 pellets	—	25377,3 s 1882 steps

pellets). For 100 pellets (125 thousand unknowns) and an accuracy of  $10^{-4}$ , the calculation time is approximately 7 hours, 1882 time steps were performed.

The displacement error was calculated as follows:

$$\varepsilon = \sqrt{\frac{\sum_i S_i \frac{(u_{r_i}^{II} - u_{r_i}^I)^2 + (u_{z_i}^{II} - u_{z_i}^I)^2}{(u_{r_i}^I)^2 + (u_{z_i}^I)^2}}{\sum_i S_i}}, \quad (31)$$

where the number  $I$  denotes a calculation with a constant step, and the number  $II$  denotes a calculation with a variable step.

For the cases of 25, 50 and 100 pellets, instead of calculating with a constant step (they were not completed due to high computational costs and the inability to estimate the maximum possible step in

Table 3: Errors with respect to the calculation with a constant step

Number of pellets	$tol = 10^{-4}$	$tol = 10^{-5}$
1 pellet	$6,72 \cdot 10^{-3}$	$2,02 \cdot 10^{-3}$
2 pellets	$9,21 \cdot 10^{-3}$	$3,59 \cdot 10^{-3}$
5 pellets	$1,97 \cdot 10^{-3}$	$1,22 \cdot 10^{-3}$
10 pellets	$4,90 \cdot 10^{-2}$	$2,51 \cdot 10^{-2}$
25 pellets	$5,15 \cdot 10^{-2}$	$2,86 \cdot 10^{-2}$
50 pellets	$6,42 \cdot 10^{-2}$	$3,53 \cdot 10^{-2}$
100 pellets	$8,36 \cdot 10^{-2}$	$4,18 \cdot 10^{-2}$

time), a calculation with a variable step was used at  $tol = 10^{-6}$ . When using a variable step, the number of time steps decreases sharply, and with the increase in the number of pellets, the errors regarding calculations with a constant step increase.

## 4 Conclusion

The formulation of the quasi-stationary problem of multicontact interaction of a system of axisymmetric thermoelastic bodies under thermomechanical loading conditions, taking into account the creep process, is presented. A numerical algorithm for solving such problems based on the mortar method is described. For the numerical solution of the problem simulating creep processes, an algorithm based on the use of the implicit Euler method is considered, the Newton method is used for linearization. The algorithm of automatic step selection based on Richardson extrapolation was applied, which made it possible to significantly increase the time steps and reduce the calculation time. Other, more complicated algorithms based on the use of artificial intelligence or neural networks can also be applied. The results of applying the introduced algorithm to solve a demonstration problem simulating some processes in a fuel element section for a mode with a constant heat dissipation power are presented. In the future, it is planned to include other significant physical phenomena in the mathematical model that must be taken into account when fully modeling fuel elements, such as pellet cracking and plasticity in the cladding.

**Acknowledgements:** The study was carried out at the expense of a grant Russian Science Foundation No. 22-21-00260, <https://rscf.ru/project/22-21-00260/>.

### Conflicts of Interest

The authors have no conflicts of interest to declare.

### References:

- [1] I.V. Stankevich, M. E. Yakovlev and Si Tu Xtet, Development of Contact Interaction Algorithm on the Basis of Schwarz Alternating Method, Herald of the Bauman Moscow State Technical University, Series Natural Sciences, Special edition: Applied Mathematics, 2011, pp. 134–141.
- [2] I. Babuska, The Finite Element Method with Penalty, Mathematics of Computation, 27, 1973, pp. 221–228.
- [3] B. I. Wohlmuth, A Mortar Finite Element Method Using Dual Spaces for the Lagrange Multiplier, SIAM Journal on Numerical analysis 38, 2000, pp. 989–1012.
- [4] T. Gustafsson, R. Stenberg, J. Videman, Error analysis of Nitsche’s mortar method, Numerische Mathematik 142, 2019, pp. 973–994.
- [5] V. S. Zarubin, G. N. Kuvyrkin, Mathematical Models of Continuum Mechanics and Electrodynamics, Bauman Moscow State Technical University, Moscow, 2008, 512 p.
- [6] N. N. Malinin, Applied Theory of Plasticity and Creep, Mechanical engineering, Moscow, 1975, 400 p.
- [7] L. A. Rozin, Variational Problem Statements for Elastic Systems, Leningrad University, Leningrad, 1978, 222 p.
- [8] T. X. Duong, L. De Lorenzis and R. A. Sauer, A segmentation-free isogeometric extended mortar contact method, Computational Mechanics 63, 2019, pp. 383–407.
- [9] P. S. Aronov, M. P. Galanin and A. S. Rodin, Application of the MSSOR for solving systems of linear equations corresponding to problems with a changing configuration of the contact surface, AIP Conference Proceedings 2448, 2021, pp. 1–12.
- [10] S. N. Korobejnikov, Nonlinear Deformation of Solids, SB RAS, Novosibirsk, 2000, 262 p.
- [11] E. Hairer, S. P. Norsett and G. Wanner, Solving Ordinary Differential Equations. Nonstiff Problems, Mir, Moscow, 1990, 512 p.
- [12] P. S. Aronov, M. P. Galanin and A. S. Rodin, Mathematical Modeling of the Contact Interaction of the Fuel Element with Creep Using the Mortar-method, KIAM Preprint.110, 2020, 24 p.
- [13] D. L. Hagman, A Library of Materials Properties for Use in the analysis of Light Water Reactor Fuel Rod Behavior, NUREG/CR-6150 TREE-1280, 1993, 445 p.

### Contribution of Individual Authors to the Creation of a Scientific Article (Ghostwriting Policy)

The authors equally contributed in the present research, at all stages from the formulation of the problem to the final findings and solution.

**Sources of Funding for Research Presented in a Scientific Article or Scientific Article Itself**  
 Funding was received for conducting this study by the Russian Science Foundation No. 22-21-00260.

**Creative Commons Attribution License 4.0 (Attribution 4.0 International, CC BY 4.0)**  
 This article is published under the terms of the Creative Commons Attribution License 4.0  
[https://creativecommons.org/licenses/by/4.0/deed.en\\_US](https://creativecommons.org/licenses/by/4.0/deed.en_US)